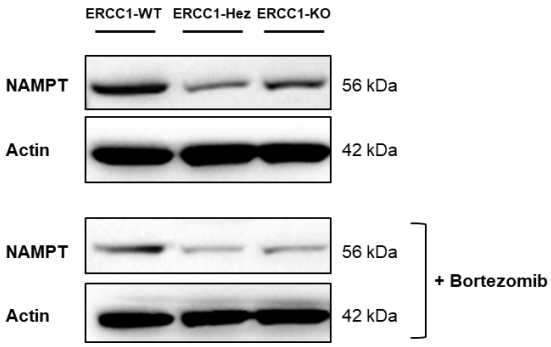

Supplementary Figure 1 – Western blot of NAMPT protein expression in A549 ERCC1-WT, ERCC1-Hez and ERCC1-KO cells. Top: control. Bottom: bortezomib exposure (48h of treatment at the IC20). Data are from one experiment.

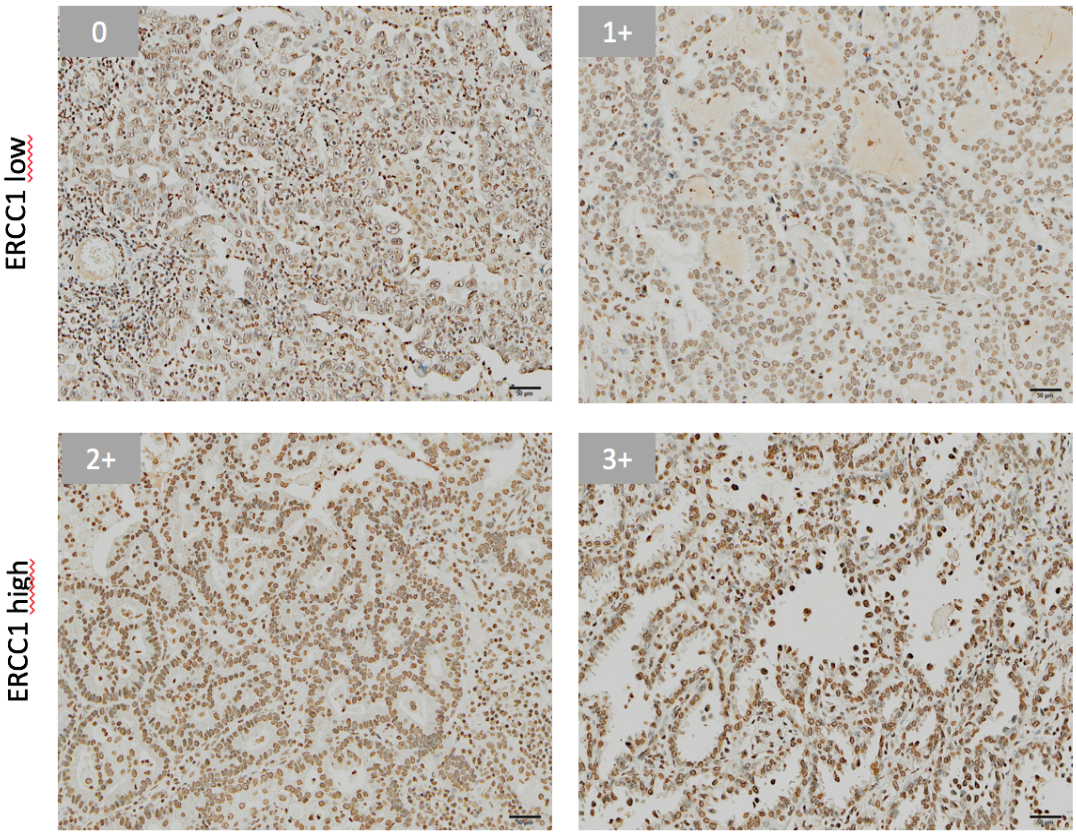

Supplementary Figure 2 – Representative images of ERCC1 staining and scoring. Scale bars: 50 µM. Data are from four representative experiments (*n* = 55 total tumor samples analyzed).

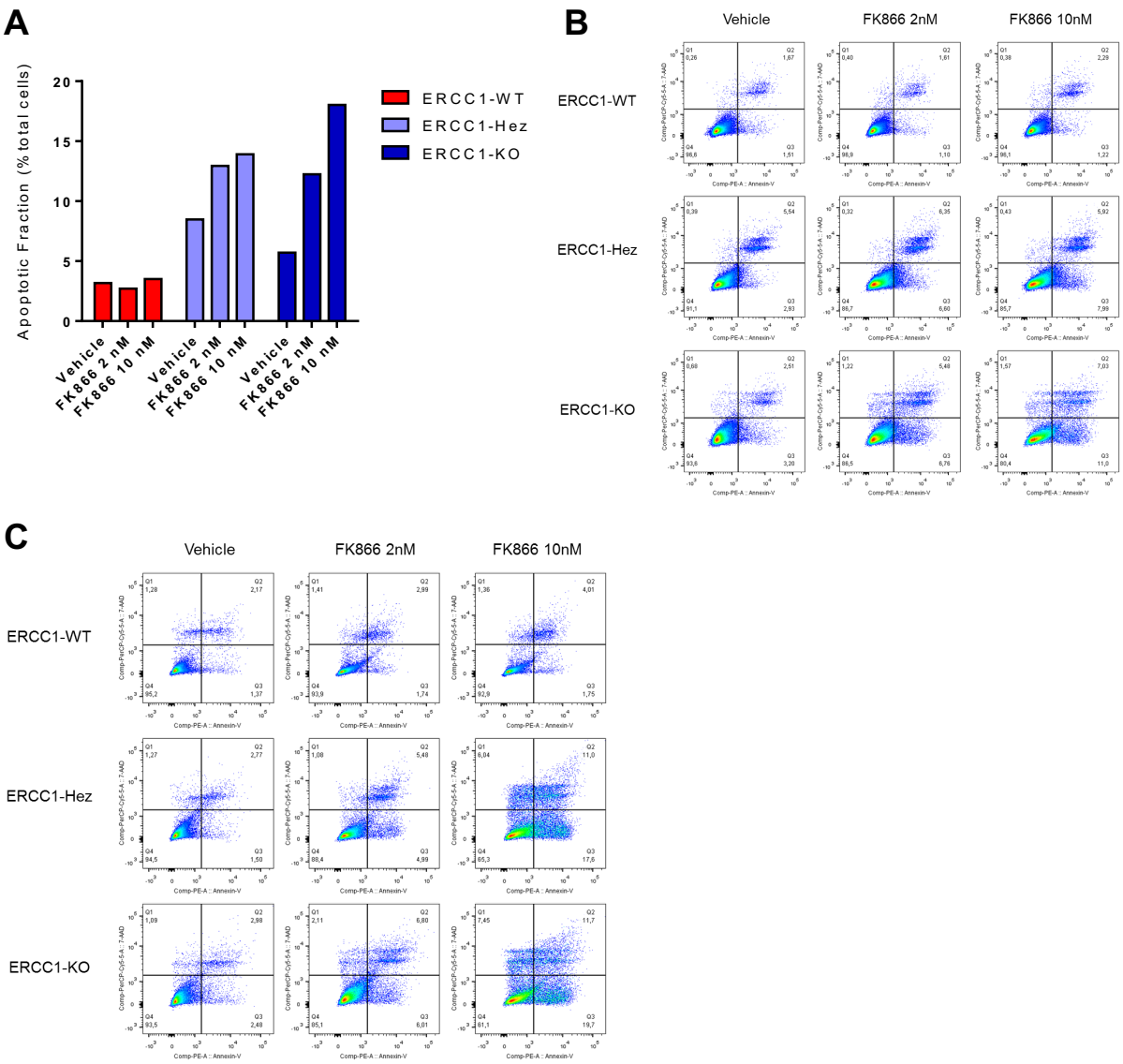

Supplementary Figure 3 – Apoptosis induction by FK866 in A549 ERCC1-proficient and ERCC1-deficient cell lines. Cells were treated with either vehicle or FK866 (2 nM and 10 nM), cultured for 3 days **(A-B)** or 5 days **(C)** and then stained with a combination of Annexin V and 7-AAD. (A) Fraction of Annexin V-positive cells after 3 days of treatment with FK866 in A549 ERCC1-proficient and ERCC1-deficient cells. **(B-C)** Dot plots of flow cytometric analysis from cells stained with AnnexinV (horizontal axis) and 7-AAD (vertical axis) after 3 **(B)** or 5 days **(C)** of FK866 exposure. Data are from one experiment

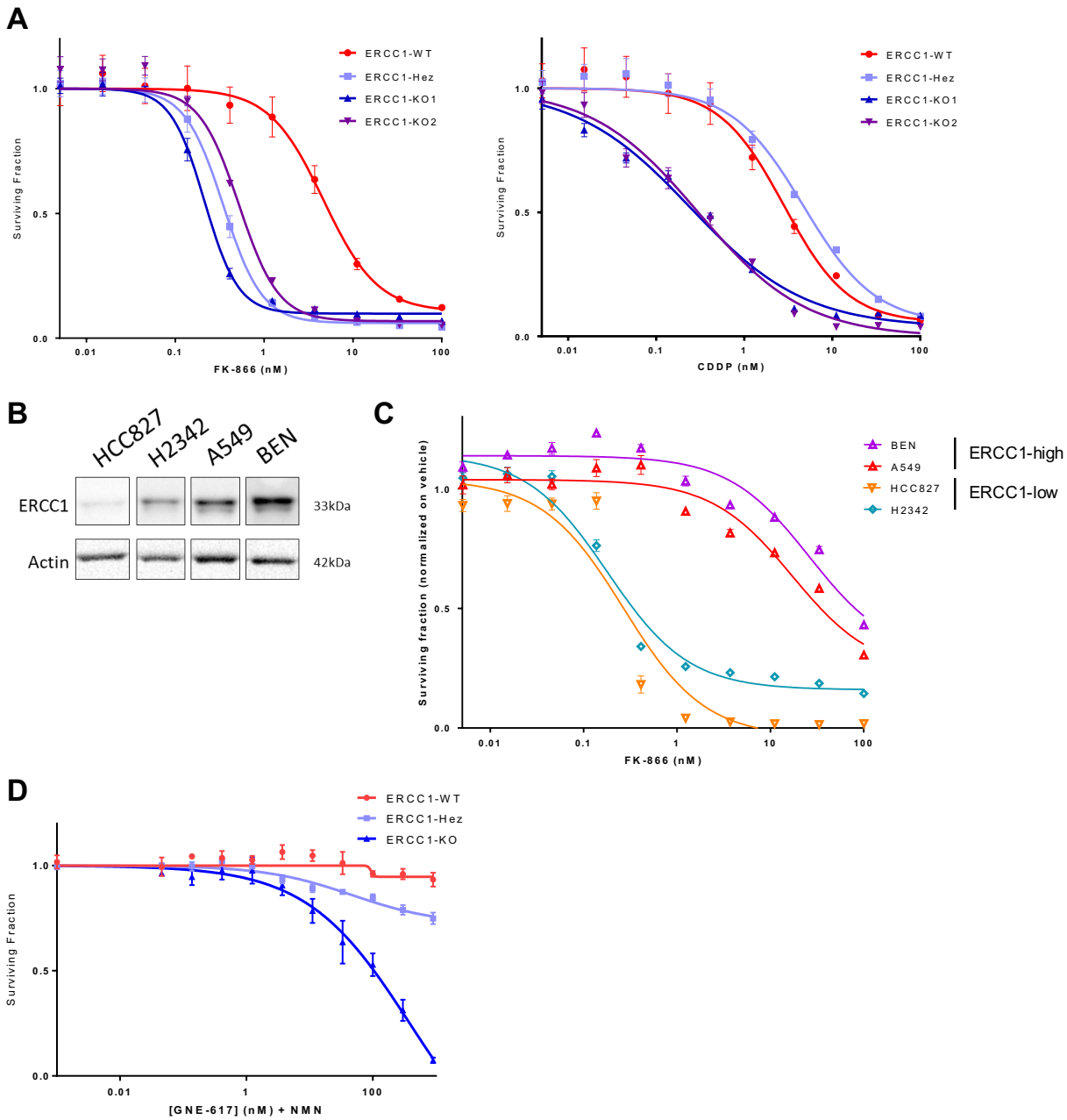

Supplementary Figure 4 – Exquisite sensitivity to NAMPT inhibition is a primary effect of ERCC1-deficiency. (A) Survival experiment on FK866 (left) and CDDP (right) of the A549 ERCC1-isogenic model. **(B)** Representative western blot of ERCC1 protein expression in the ERCC1 non-isogenic NSCLC models. Data are from one experiment. **(C)** Survival curves assessing sensitivity to FK866 assessed by short-term assay in the ERCC1 non-isogenic NSCLC models. Data are from one representative experiment. **(D)** Rescue of the GNE-617 toxicity by the administration of nicotinamide mononucleotide (NMN) 100 µM in A549 cells. For **(A,C,D)** data represents mean surviving fraction ± SEM from one of three independent experiments.

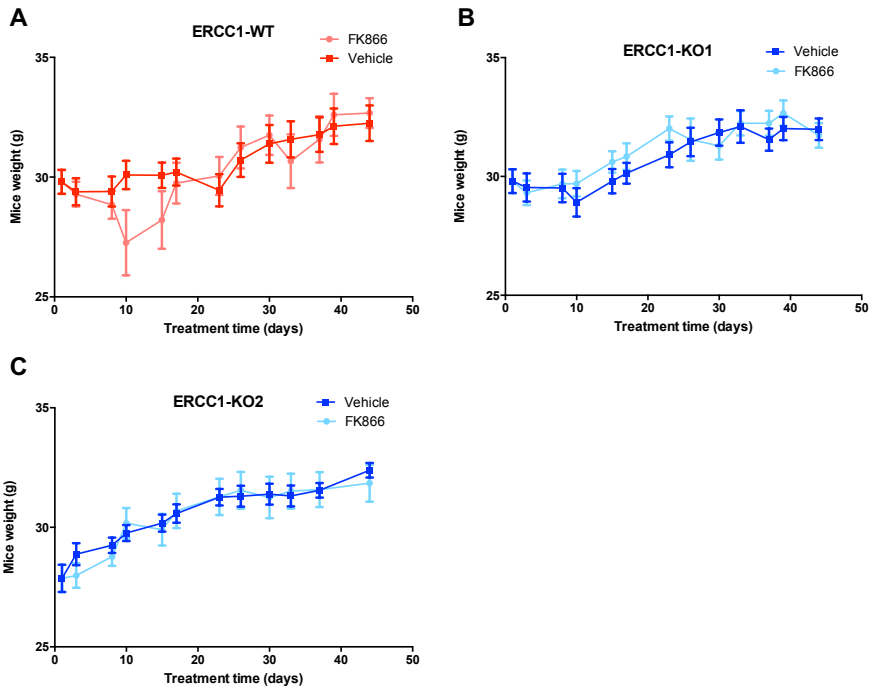

Supplementary Figure 5 – In vivo supplementary data. (A-C) Mice weights during treatment with vehicle or FK866, in groups injected with the ERCC1-WT cells **(A)** and ERCC1-KO isogenic cell lines **(B-C)**. Data are mean ± SD with n = 8 mice in each group.

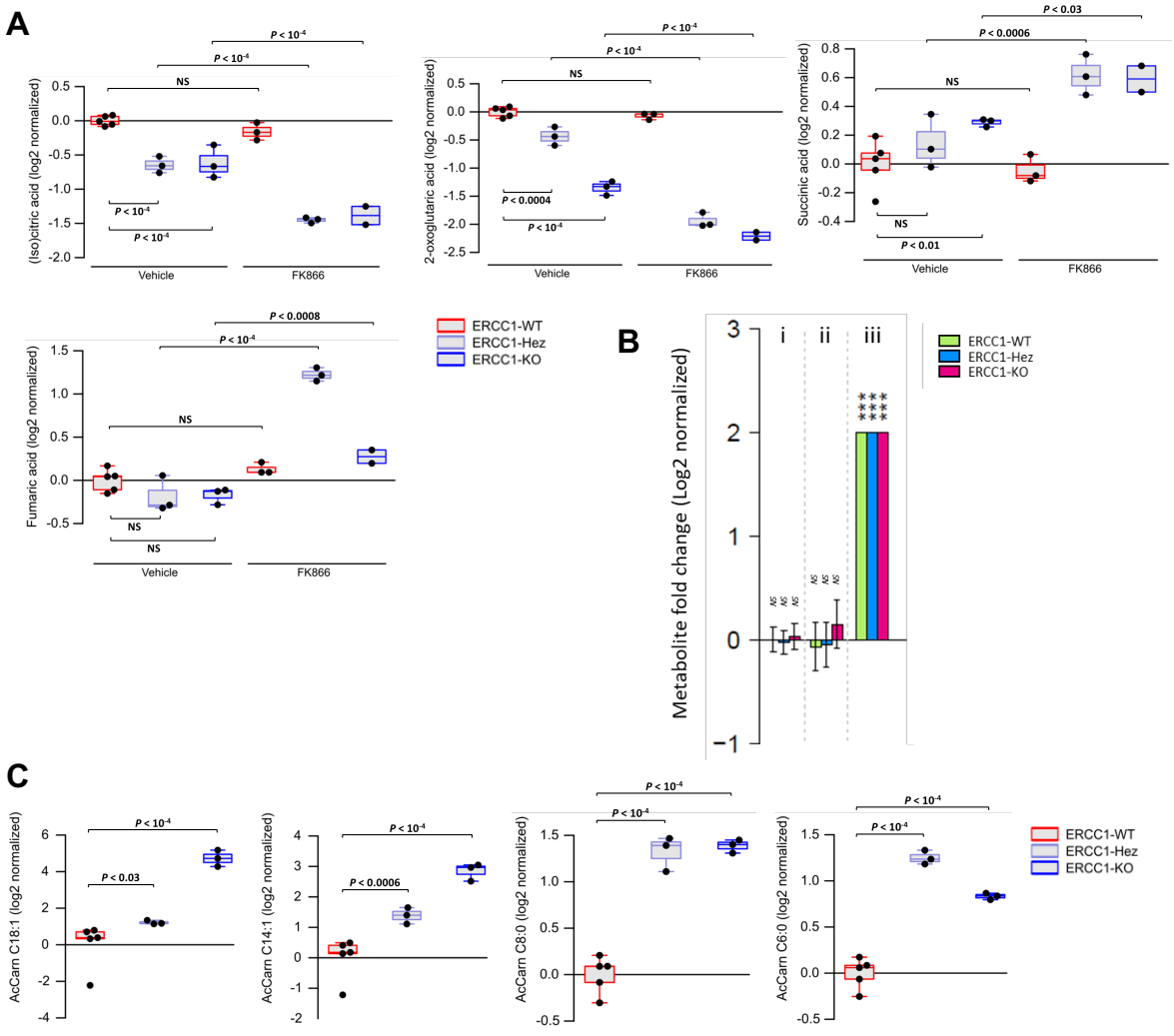

Supplementary Figure 6 – Supplementary metabolomic data (1). (A) Distribution of the relative abundancies of citrate/isocitrate, 2-oxoglutarate, succinate and fumarate across the ERCC1-WT (n = 5 independent samples), ERCC1-Hez (n = 3) and ERCC1-KO (n = 3) cell lines treated with FK866 or vehicle. **(B)** Measurements of succinate (i), fumarate (ii) and methylmalonic acid levels (iii) levels following inhibition of the succinate dehydrogenase by 24h treatment with methylmalonic acid in A549 ERCC1-proficient and ERCC1-deficient cell lines. Abbreviations: NS, not significant; ***, $P < 0.01$. **(C)** Distribution of the relative abundancies of C18:1, C14:1, C8:0 and C6:0 acylcarnitines across the ERCC1-WT, ERCC1-Hez and two ERCC1-KO cell lines treated by vehicle. For **(A-C)** statistical analyses and data representation were performed on pre-processed, log2-transformed and imputed data and reported as such without back-transformation. Moderated statistics were used for differential analysis. Moderated statistics were used for differential analysis. Levels of significance were denoted as P-values adjusted according to Benjamini and Hochberg to control the false discovery rate (FDR).

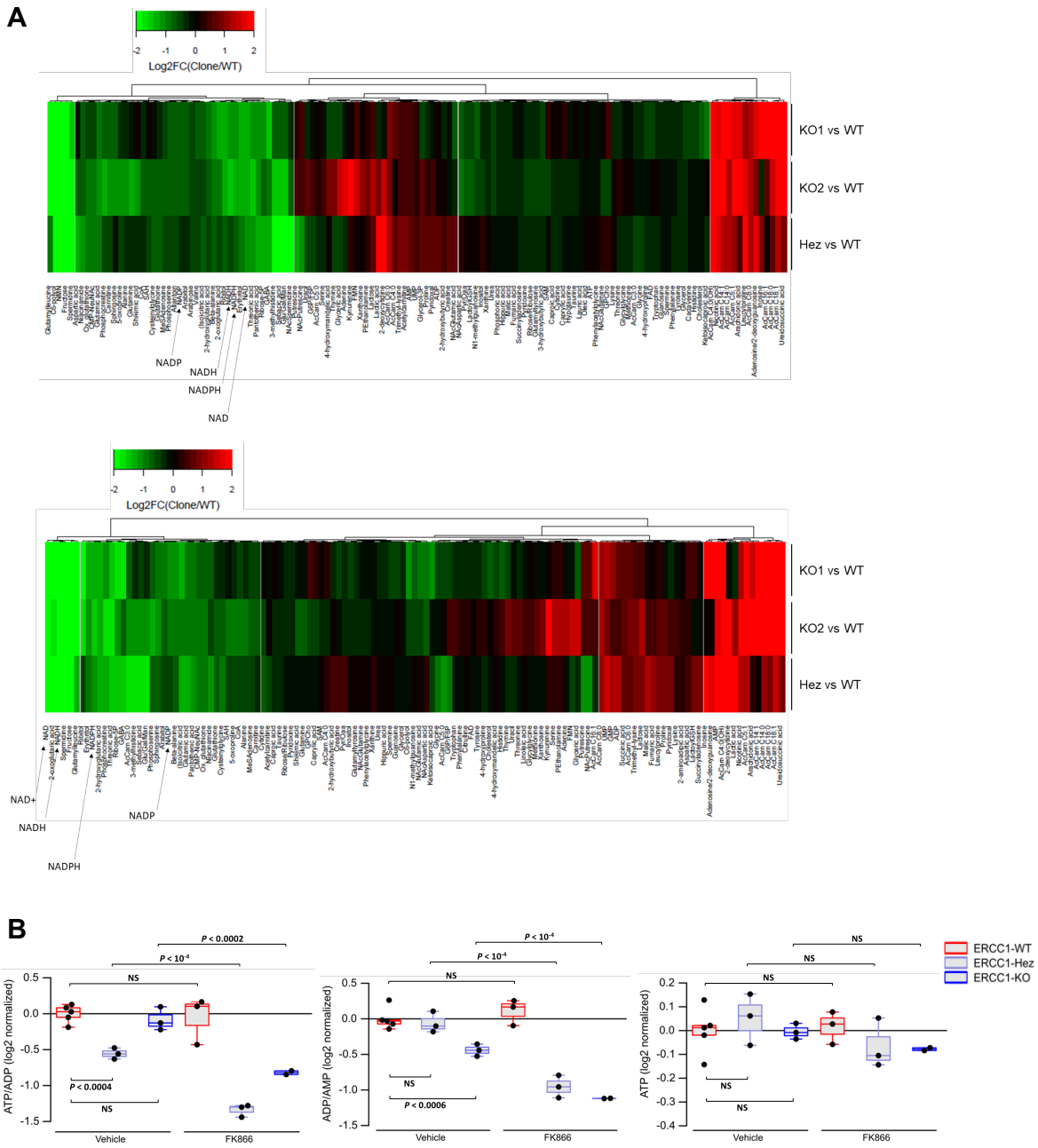

Supplementary Figure 7 – Supplementary metabolomic data (2). (A) Relative distribution of metabolites in the ERCC1-Hez (n = 3 independent samples) and two ERCC1-KO (n = 3 per group) cell lines treated by vehicle (top) or FK866 (bottom). Data are normalized on the ERCC1-WT vehicle (top) or FK866 (bottom) groups. Metabolites at FDR < 0.1 (Benjamini and Hochberg) are depicted. Selected metabolites from the NAD biosynthesis pathway are highlighted. **(B)** Distribution of the relative abundancies of ATP, ATP/ADP and ATP/AMP ratios across the ERCC1-WT (n = 5 independent samples), ERCC1-Hez (n = 3) and ERCC1-KO (n = 3) cell lines treated with FK866 or vehicle. Data were centered on the ERCC1-WT vehicle group for comparative purposes. For **(A-B)** statistical analyses and data representation were performed on pre-processed, log2-transformed and imputed data and reported as such without back-transformation. Moderated statistics were used for differential analysis. Levels of significance were denoted as P-values adjusted according to Benjamini and Hochberg to control the false discovery rate (FDR).

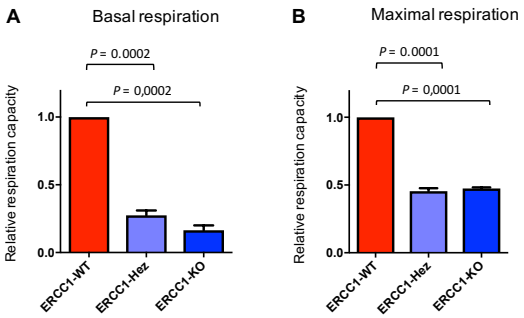

Supplementary Figure 8 – ERCC1 deficiency associates with decreased respiratory capacity. (A–B) Relative basal **(A)** and maximal **(B)** mitochondrial respiratory capacity of intact A549 ERCC1-WT, ERCC1-Hez and ERCC1-KO cell lines measured in real time with high-resolution respirometry (Oroboros). Data represents mean respiration capacity ± SD normalized to the ERCC1-WT group with $n = 3$ independent samples per group. Statistical analyses are indicated (one-way ANOVA adjusted for multiple comparisons).

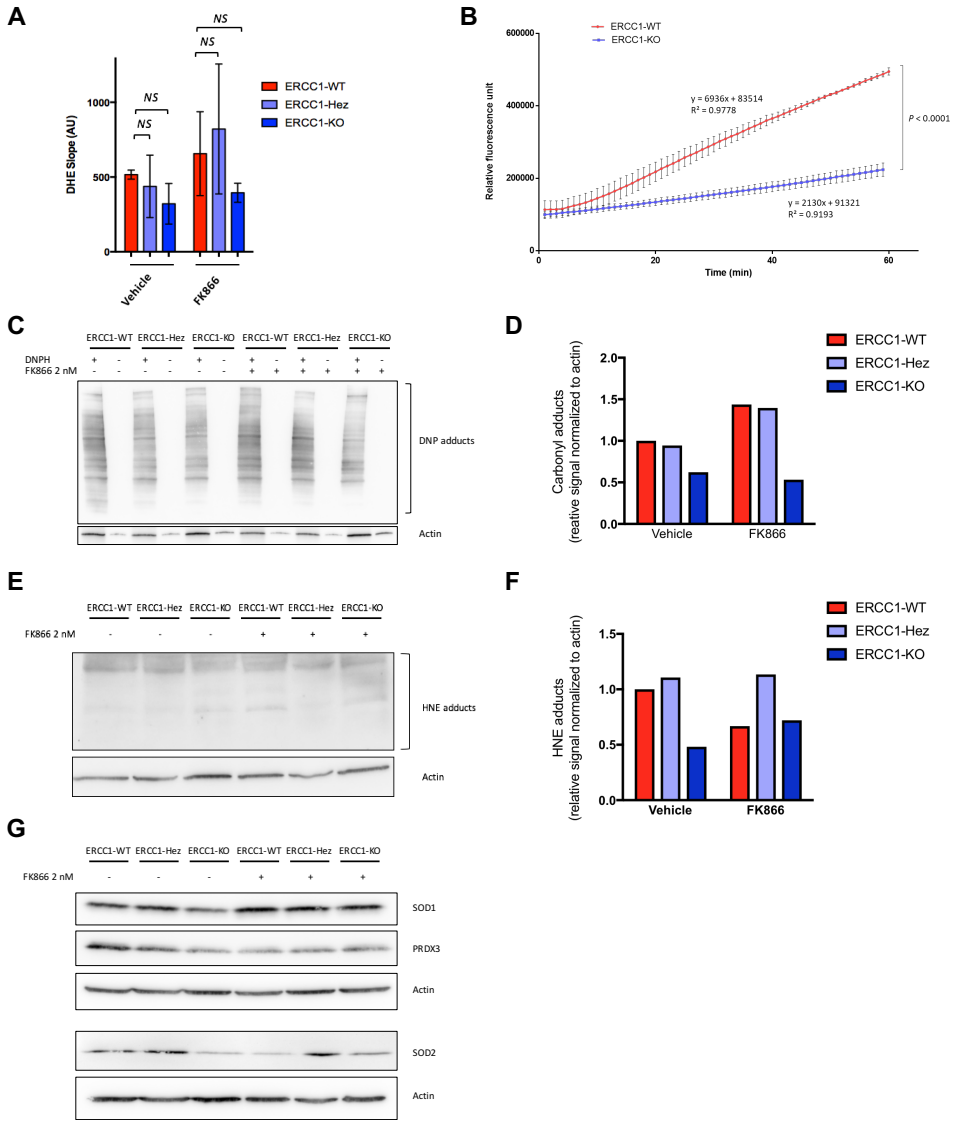

Supplementary Figure 9 – ERCC1-deficient cells do not have increased ROS levels. (A) Reactive oxygen species (ROS) kinetics were measured using the kinetics of dihydroethidium (DHE) fluorescence in A549 ERCC1-proficient and ERCC1-deficient cell lines. Data represent mean DHE slope ± SD from two independent experiments. Statistical analyses are indicated (Friedman test adjusted for multiple comparisons using Dunn's test). NS: no statistically significant difference. **(B)** Extracellular H2O2 kinetics in ERCC1-proficient and ERCC1-deficient models. Data represent mean ± SD from one of two independent experiment. Statistical analyses are indicated (linear regression analysis). **(C)** Western blot of carbonyl adducts in A549 ERCC1-proficient and ERCC1-deficient cell lines (Oxyblot procedure). Each sample is followed by its replicate without DNPH derivation as negative control. DNP: dinitrophenyl hydrazone adducts, DNPH: 2,4-dinitrophenylhydrazine. **(D)** Quantification of carbonyls adducts measured by western blot in A549 ERCC1-proficient and ERCC1-deficient cell lines. **(E)** Western blot of HNE adducts in A549 ERCC1-proficient and ERCC1-deficient cell lines. HNE: 4-Hydroxynonenal. **(F)** Quantification of HNE adducts measured by western blot in A549 ERCC1-proficient and ERCC1-deficient cell lines. **(G)** Western blot of SOD1, SOD2 and PRDX3 protein expression in A549 ERCC1-proficient and ERCC1-deficient cell lines. SOD1: superoxide dismutase 1, SOD2: superoxide dismutase 2, PRDX3: peroxiredoxine 3. For **(C-G)**, data are from one experiment.

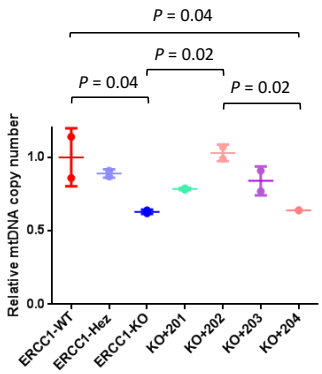

Supplementary Figure 10 – ERCC1 deficiency associates with decreased mitochondrial biogenesis. Relative mitochondrial DNA (mtDNA) copy number in A549 ERCC1-WT, ERCC1-Hez, ERCC1-KO, and ERCC1-rescued (isoforms 201 to 204) cell lines. Values were normalized to ERCC1-WT cells. Statistical analyses are indicated (one-way ANOVA adjusted for multiple comparisons). Only statistically significant differences are depicted, all other *P*-values are not significant. Data are from two independent experiments**.**

Supplementary Methods

Protein extraction for immunoblotting. Proteins were extracted in lysis RIPA buffer (50 mM Tris, 150 mM NaCl, 5 mM EDTA, 0.5% sodium deoxycholic acid, 0.5% NP-40, 0.1% SDS) supplemented with protease inhibitor cocktail (Roche Molecular®). For the Oxyblot procedure, samples were prepared in RIPA buffer with 50 mM DTT and 1 mM PMSF. Proteins were incubated with 2,4-dinitrophenylhydrazine (DNPH) to form the 2,4-dinitrophenyl (DNP) hydrazone derivatives. For Hydroxynonenal (HNE) quantification, samples were prepared using Laemli.

Protein extraction for SILAC. Cells were grown in SILAC DMEM supplemented with either isotope-labeled (Lys 8, Arg 10) or unlabeled amino acids for eight doubling times. After protein extraction and quantification, equal concentration of labeled and unlabeled lysates were mixed together and processed according to previously published methods (1). Briefly, 1 ml of mixed lysate, equivalent of 1-1.5mg total lysate was mixed with 8ml of 8M Urea (UA) buffer and was loaded into an Amicon Ultra 15 Ultracel 30k device, with a 1:8 lysis buffer to UA ratio. After concentrating twice at 4000g for 30 min in 10 mL of UA, samples were incubated in darkness in 2mL of IAA at RT for 30 min, prior to 15 min centrifugation (4000g). After further concentration in UA, samples were washed twice with 1ml of 50mM Ammonium Bicarbonate (ABC) buffer. The filter was put onto a new tube and trypsin was added (1:100 of the lysate amount) in 1 mL of ABC. Digestion was conducted overnight at 37°C in a wet chamber. Peptides were collected by centrifugation (15 min), prior to adding 0.5 mL of ABC and spinning for 15 min, followed by adding 0.5ml of 20% Acetonitrile in ABC. Extracts were acidified and desalted on a C18 cartridge (Sep-Pak), prior to off-gel isoelectric focusing using a 3100 Off-Gel Fractionator® (Agilent

Technologies).

SILAC proteomic analysis. Twenty percent of each sample was analyzed as a 6µl injection, including a known spiked concentration of a three- peptide mixture QC sample spike. Peptides were resolved on a 75µm I.D. 15 cm C18 packed emitter column (3µm particle size; NIKKYO TECHNOS CO., LTD, Tokyo, Japan) over 120 min SET 1 (runs 1 and 2 only) or 90min using a non-linear gradient of 96:4 to 50:50 buffer A:B (buffer A: 2% acetonitrile / 0.1% formic acid; buffer B: 80% acetonitrile / 0.1% formic acid) at 250nl/min. Peptides were ionized by electrospray ionization using 1.8kV applied immediately pre-column via a microtee built into the nanospray source. Sample was infused into an LTQ Velos Orbitrap mass spectrometer® (Thermo Fisher Scientific, Hemel Hempstead, UK) directly from the end of the tapered tip silica column (6-8 µm exit bore). The ion transfer tube was heated to 200°C and the S-lens set to 60%. MS/MS were acquired using data dependent acquisition based on a full 30,000 resolution FT-MS scan with preview mode disabled and internal lock mass calibration against the polysiloxane ion at 445.120025 m/z. The top 20 most intense ions were fragmented by collision-induced dissociation and analyzed using normal ion trap scans. For sample set 2, the top 10 ions were also fragmented and analyzed using enhanced ion trap scans. Automatic gain control was set to 1,000,000 for FT-MS and 30,000 for IT-MS/MS, full FT-MS maximum inject time was 500ms and normalized collision energy was set to 35% with an activation time of 10ms. Wideband activation was used to co-fragment precursor ions undergoing neutral loss of up to -20 m/z from the parent ion, including loss of water/ammonia. MS/MS was acquired for selected precursor ions with a single repeat count followed by dynamic exclusion with a 10ppm mass window for 60s (120 min gradient) (SET 1 only) or 45s (90 min gradient) based on a maximal exclusion list of 500 entries.

Metabolomics analysis. Prior to LC-MS/MS, pure standard of NMN was infused to optimize the MRM transitions enabling its quantification together with 14 other metabolites: Q1=335.1 and Q3=123.1 with the fragmentor and the collision energy set at 100eV and 20eV. Profiles generated by the three methods were combined in the statistical environment R (http://www.R-project.org/) for data processing, peak annotation, data reduction and statistical treatment. After quality control checks and the exclusion of redundant metabolites, the final dataset comprises 1947 features that can be classified according to the recommendations of the Metabolomics Society for metabolite annotation as follows: 159 as level 1, 238 as level 2 and 1550 as level 4. In the article, reporting and interpretation of the metabolomics profiles were only presented for the 159 level 1 features: 70 were obtained by metabolomics open profiling and 10 and 79 quantified by targeted LC-MS/MS and GC-MS/MS methods. All statistical analyses and data representation were performed on pre-processed, log2-transformed and imputed data (2) and reported as such without back-transformation. Moderated statistics were used for differential analysis (3). Levels of significance were denoted as p-values when in their raw form or as FDR when adjusted according to Benjamini and Hochberg (4) to control the false discovery rate (FDR).

Respiration analyses. For Seahorse technique, proliferating A549 ERCC1-WT, ERCC1-Hez and ERCC1-KO cells were seeded in Seahorse XF-96 cell culture microplates in six replicates at 20,000 cells/well. After 24h, cells were washed with unbuffered XF Assay Medium (pH 7.4, 25 mM glucose) 1h prior to measurement. Indices of glycolysis and mitochondrial function were measured after sequential injections of oligomycin (1µg/ml final), CCCP (first 0,25 µM then 0,50 µM) and antimycin A (1µg/ml). For high-resolution respirometry with the Oroboros "O2k" device

(www.oroboros.at/), cells were suspended in culture medium. Respiration at 37°C was measured in the basal state and after successive addition of 1 µg/mL oligomycin once, 1,25 µM CCCP four times (until reaching maximal respiration at a final 5 µM CCCP), and 1 mM potassium cyanide once. Oxygen consumption rates were calculated by Datlab 4® software and normalized to the number of cell/ml. Experiments were performed in duplicates. In both cases, the respiration linked to ATP production was calculated as the difference in oxygen consumption before and after injection of oligomycin. The maximal respiratory capacity was determined by subtracting the non-respiratory oxygen consumption (under cyanide) from the maximal oxygen consumption obtained with CCCP.

Gene expression and mtDNA content analysis by qPCR. For NAMPT gene expression analysis, cDNA was synthetized using the Roche® Transcription First Strand cDNA Synthesis (04379012001) after RNA extraction using the QIAGEN® RNeasy Micro kit (74004), according to the manufacturer's protocol. Real-time PCR amplification was performed on 200 ng of total cDNA using the ViiA™ 7 Real-Time PCR System (Applied Biosystems) and the Taqman® Gene Expression Assay (4440038) according to the manufacturer's protocol. NAMPT probe was purchased from ThermoFisher Scientific® (Hs00237184_m1). GAPDH (Hs03929097_g1) and Beta-2-microglobulin (B2M) (Hs99999907_m1) were used as endogenous reference. Quantification of mtDNA was performed as described (6). Real-time PCR amplification was performed on 200 pg of total DNA using the ViiA™ 7 Real-Time PCR System (Applied Biosystems®) and Power Sybr Green PCR Master mix (Applied Biosystems®) according to the manufacturer's protocol. The region tested on mtDNA was included in the 12S gene (forward primer: CGCCAGAACACTACGA; reverse primer: AGGGTTTGCTGAAGAT) (10). The

nuclear encoded 18S rRNA gene was used as endogenous reference (forward primer: AAACGGCTACCACATCC; reverse primer: CCTCGAAAGAGTCCTG) (5). The level of mtDNA was calculated using the ΔCT of average CT of mtDNA and nDNA (ΔCT = CT nDNA - CT mtDNA) as $2^{\Delta CT}$ (6).

Mitochondrial Surface Estimation. Representative pictures from ERCC1-WT (20 pictures) and ERCC1-KO (27 pictures) cells were taken with a SISMegaviewIII charge-coupled device camera (Olympus, Tokyo, Japan). Mean surface was calculated after manual delimitation of mitochondria from ERCC1-WT (n=87) and ERCC1-KO (n=122) cells. Student's t-test was used to determine the significance of the differences between the mean mitochondrial surfaces in both cell lines.

Immunohistochemisty on tumor samples. Archival samples from resected lung adenocarcinoma (stage I, II and IIIA) were used. For each case, one representative formalin fixed paraffin embedded (FFPE) block was selected for the study. Automated immunohistochemistry was performed on 4 μm thick sections from FFPE tissue blocks using a Ventana Discovery Ultra platform (Roche Diagnostics®, Tucson, AZ). After deparaffinization and epitope retrieval (CC1 buffer, 32 minutes), the slides were incubated with an anti-ERCC1 (clone SP68, Spring Bioscience®, 1:500 dilution) or an anti-NAMPT (clone 14A5, Merck Millipore, 1:1000 dilution) antibody during one hour at room temperature. Detection was performed with the UltraMap detection kit and diaminobenzidine as a chromogen. Pathological assessment of NAMPT and ERCC1 stains were performed independently by a senior pathologist. ERCC1 immunohistochemistry was scored as high or low based on the prominent intensity of staining observed for each case in the nuclei of tumor cells. Tumors with weak staining (0/1+) were scored as low and tumors with strong staining

(2+/3+) was scored as high. Staining of intratumoral lymphocytes was used as an internal positive control. Scoring was based on cytoplasmic staining for NAMPT using an H-score (staining intensity from 0 to 3+ multiplied by percentage of positive cells).

Apoptosis. Apoptosis was assessed through the detection of cell surface phosphatidylserine exposure, using phycoerythrin-conjugated Annexin V staining (PE Annexin V Apoptosis Detection Kit, Becton Dickinson®) and flow cytometry analysis. Cells were cultured with vehicle or 2 and 10 nM FK866, and collected following 5 days treatment. 5.10^5 cells were collected per sample, washed twice and suspended in the provided binding buffer, containing 5% Annexin V and 5% 7-AAD. Detection was achieved using a fluorescent-activated cell sorter LSR-II flow cytometer (Becton Dickinson®), running FACS Diva software®. Data analysis were performed using FlowJo software®.

ROS production. Dihydroethidium (DHE) fluorescence kinetics were measured using flow cytometry during 30 minutes without treatment and on FK866 at 2 nM. Antimycin, a complex III inhibitor that induces a major oxidative stress, was used as a positive control at 1 µM. Extracellular H2O2 production was measured using the Amplex red/horseradish peroxidase (HRP) assay. Amplex Red peroxidation was monitored continuously for 1 hour. All measurements were performed in triplicate.

Supplemental Methods References

1. Wiśniewski JR, et al. Universal sample preparation method for proteome analysis. Nat Methods. 2009;6(5):359–62.

2. Kim H, Golub GH, Park H. Missing value estimation for DNA microarray gene expression data: local least squares imputation. Bioinformatics. 2005;21(2):187–198.

3. Ritchie ME, et al. limma powers differential expression analyses for RNA-sequencing and microarray studies. Nucleic Acids Res. 2015;43(7):e47.

4. Benjamini Y, Hochberg Y. Controlling the false discovery rate: a practical and powerful approach to multiple testing. J R Stat Soc Series B Stat Methodol. 1995;57(1):289–300.

5. Suissa S, et al. Ancient mtDNA genetic variants modulate mtDNA transcription and replication. PLoS Genet. 2009;5(5):e1000474.

6. Chatre L, et al. Reversal of mitochondrial defects with CSB dependent serine protease inhibitors in patient cells of the progeroid Cockayne syndrome. Proc Natl Acad Sci U S A. 2015;112(22):E2910–E2919.